ISSN 1561-9087 Прикладна гідромеханіка. 2015. Том 17, N 4. С. 58 – 64

УДК 532.012.2

HYDRODYNAMIC TESTING OF FLEXIBLE PROFILES FOR A VERTICAL AXIS TURBINE

D. N. ZEINER-GUNDERSEN*, S. A. S. ZEINER-GUNDERSEN**

**Smieveien 19, 3470 Slemmestad, Norway*
***Hamangskogen 49, 1338 Sandvika, Norway*

Отримано 07.09.2015

Hydrodynamic turbine functionality depends on the ability of the individual profiles to capture the water energy efficiently during rotation. Here, we describe a unique flexible profile design based on hydrodynamic thrust characteristics inspired by swimming and flying creatures. The concept was based on a flexible double cambered profile that would have a relatively high lift to drag ratio independent of the rotational azimuth position in a vertical axis hydrodynamic turbine application. In order to establish the design of a profile to be implemented into a vertical axis turbine, several different flexible profile models were tested in a cavitation tunnel with controlled water flow dynamics, and their lift, drag, and momentum characteristics were established. Three different diameters of the leading edge rod/profile were tested: 20, 30, and 40 mm corresponding to thickness ratios of 7%, 10%, and 13%, respectively. The material characteristics of the flexible fabric used in the tests had positive features with respect to marine propulsion, unwanted marine growth on its surface, flexibility, and low coefficients of friction.

KEY WORDS: flexible profile turbine, hydrodynamics, cascade model

Гідродинамічна функціональність турбіни залежить від властивості кожного профіля захоплювати енергію води під час обертання. Ми описуємо унікальний дизайн гнучкого профіля, який базується на характеристиках гідродинамічної тяги, подібної до тої, яка використовується плаваючими та літаючими живими істотами. Концепція полягає у використанні гнучкого профіля подвійної кривизни, який має відносно високе відношення піднімальної сили до сили опору незалежно від позиції по куту обертання, в застосуванні для гідродинамічних турбін з вертикальною віссю. Для розробки дизайну профіля, яких буде використовуватися у вертикальній турбіні, декілька моделей гнучких профілів було протестовано у кавітаційному каналі з керованою динамікою потоку, та було виміряно піднімальні сили, сили опору та моменти обертання. Три різних діаметри передньої кромки було досліджено: 20, 30 та 40 мм, що відповідають відношенню товщин 7%, 10% и 13%. Фізичні характеристики гнучкого матеріалу покриття профіля, який використовувався в тестах, мають позитивні властивості по відношенню до створення тяги, небажаного росту колоній морських мікрорганізмів на його поверхні, гнучкості та низького коефіцієнту опору.

КЛЮЧОВІ СЛОВА: гнучкий профіль турбіни, гідродинаміка, каскадна модель

Гидродинамическая функциональность турбины зависит от способности каждого профиля захватывать энергию воды во время вращения. Здесь мы описываем уникальный дизайн гибкого профиля, основанный на характеристиках гидродинамической тяги, подобной используемой плавающими и летающими живыми существами. Концепция основывается на гибком профиле двойной кривизны, который имеет относительно высокое отношение подъемной силы к силе сопротивления независимо от положения по углу вращения, в применении для гидродинамических турбин с вертикальной осью. Для выработки дизайна профиля, который будет использован в турбине с вертикальной осью, несколько моделей гибких профилей были протестированы в кавитационном тоннеле в управляемой динамикой потока, и были измерены их подъемные силы, силы сопротивления и моменты вращения. Три различных диаметра передней кромки были исследованы: 20, 30 и 40 мм, соответствующие отношению толщин 7%, 10% и 13%. Физические характеристики гибкого материала покрытия профиля, использованного в тестах, имеют позитивные свойства по отношению создания тяги, нежелательного роста колоний морских микроорганизмов на его поверхности, гибкости и низкого коэффициента трения.

КЛЮЧЕВЫЕ СЛОВА: гибкий профиль турбины, гидродинамика, каскадная модель

INTRODUCTION

A novel vertical axis turbine with flexible profiles has been designed to optimize energy capture from hydrodynamic environments (Zeiner-Gundersen, MS1 and MS2). Because of the flow complexity and rotational behavior of a hydrodynamic vertical axis turbine, combined with the possibility for high yield, it was important to first create a novel profile design. Studies have shown the beneficial effects of structural flexibility in the generation of lift and propulsive forces, often increasing propulsion efficiency [1 – 5]. The profile's geometric configuration determines its hydrodynamic characteristics. The design could beneficially incorporate a double-cambering effect for high yield, the flexibility to adjust to various induced local flow velocities, and the ability to maintain a high lift/drag ratio over a large range of angle of attacks. In particular, these aspects are important for a good design with low tip speed ratios, which cause significant variation in angle of attack versus rotational azimuth angle.

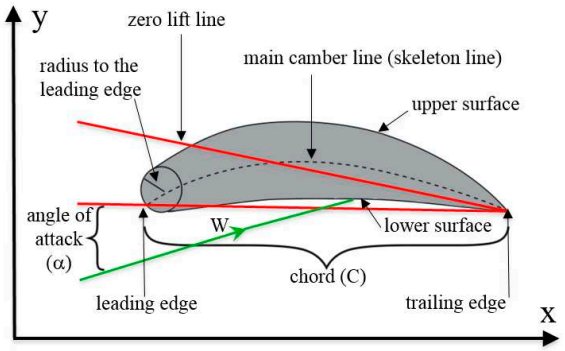

Fig. 1. Two-dimensional wing section with general profile characteristics

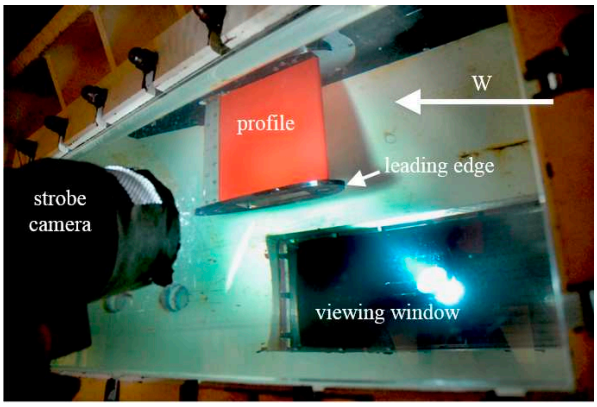

Fig. 2. A typical model profile mounted on the six-component balance in the measurement section of the cavitation tunnel, with a strobe flash camera used for documentation. W = relative water flow. Scale bar = 10 cm.

Fig. 1 shows a typical cross section of a profile. The main characteristic of the profile is the mean curvature line (main camber line or skeleton line), which is located halfway between the upper and lower surface of the profile. The size of the radius at the leading edge influences the boundary separation characteristics around the profile section. The shape of the main camber line is important when determining the aerodynamic/hydrodynamic characteristics of a profile. Typically, profiles with curvatures in a subsoundstream will generate lift even if the angle of attack is zero, while profiles with symmetrical upper and lower edges (so that the curvature is zero) have zero lift at 0° angle of attack [6,7]. Positive curvature will increase the lift, but significant increases also induce boundary layer separation that destroys the lift even at low speed. Therefore, a hydrodynamic design objective is to balance and maximize lift while avoiding boundary layer separation. The curvature, shape, and thickness of a profile will further give combined lift and torque characteristics. The angle of attack affects the position of the aerodynamic center of the wing profile. Typically, for a slim profile in subsoundspeed, this should be located at 1/4 the chord line length from the leading edge.

The total resistance is determined by (i) the overall hydrodynamic shape, surface, and front configuration of the profile, (ii) angle of attack, and (iii) water speed and density. In order to create lift, the pressure on the underside of the leading edge of the profile must be greater than on the upper side, and the water flow speed must be greater on the upper side (with water flow equal on both sides at the trailing edge). The resistance force (drag) is derived from the viscous fluid flows around the profile. The pressure at the front (leading edge) of the profile is higher than behind the profile and acts parallel to the relative inflow water velocity. Surface friction is caused by the sub fluid layer, which is very close to the profile surface and is virtually still. The viscosity of such a stagnant layer will affect the fluid flowing further out from the profile, creating a boundary layer at the surface.

An increased angle of attack will eventually separate flow over the profile, starting at the trailing edge and moving forward. With large induced angles of attack, the separation moves up to the leading edge of the profile, which leads to reduction in the profile lift, and can give imbalanced turbine rotation, and decreased turbine efficiency. Dynamic stall occurs with a rapid change in angle of attack, resulting in disordered turbulence passing over the low-pressure side of the lift wing. A vortex is shed from the leading edge backwards above the profile, eventually reducing lift and inducing stall once the vortex passes behind the trailing edge. Flexible profiles will dampen the release of sharply generated vortices and adjust the profile to the angle of attack versus azimuth position during turbine rotation, thus relatively reducing the effect of dynamic stall and occurrences.

A series of hydrodynamic tests was performed on various hydrodynamic scaled models of selected flexible profiles in order to ensure that the full-scale vertical axis turbine was designed based on sound engineering principles. The tests established the lift, drag, and momentum characteristics of the profiles for various angles of attack, enabling the selection of an optimal hydrodynamic profile to be used in the full-scale turbine design.

1. PROFILE MODEL DESIGN

The profile models were designed and manufactured to an interface specification given by SSPA (Chalmers University, Gøteborg, Sweden) in order to fit into an existing six-component balance unit (R41) within a cavitation tunnel. The profile models were attached to a six-component balance mounted in a window at the top of the measurement section in the cavitation tunnel (fig. 2). Fig. 3 shows the typical model profile design. Some of the profile subcomponents were manufactured by 3D printing.

The tested profiles were made with different configurations and in general surrounded by an armored flexible plastic fabric (pre-stretched flexible polyvinyl chloride-coated nylon fabric with high tear strength). The flexible material was optimized for the following design parameters: coefficient of fluid-friction, friction associated with it's operating functionality, skin friction, internal friction, water velocity, weight to size ratio of the wing, deformation over time, tear strength, plane flexibility, surface patterning and thickness. To ensure proper functionality and reduce material fatigue, experiments determined that the friction had to be held at a minimum. The material specifications to be utilized in future large-scale turbine designs are proprietary information and will not be presented in this paper.

The various profile configurations were mounted onto a steel frame with four main parts: a rod at the leading edge, a 40 mm clamp at the trailing edge, and two flanges, one on each side. The flanges supported the leading edge rod and the trailing edge clamp, and the upper flange was connected to the six-component balance unit through an interface connection. The clamping device at the trailing edge allowed for variation of the tension in the fabric. All of the profile models were equipped with a Perspex glass window in the bottom for visualization of profile dynamics. In some configurations, the leading edge was equipped with a nose. In the last round of tests, $\sim$ 30 mm threads were mounted on the foils to visualize the flow (fig. 3).

Three different diameters of the leading edge rod/profile were tested: 20, 30, and 40 mm corresponding to thickness ratios of 7%, 10%, and 13%, respectively. The recommended maximum span was 350 mm in order to avoid excessive forces on the six-component force measurement unit.

To reduce the influence of drag-induced wingtip vortices, the test wings were equipped with winglets. A reduction in drag was observed during tests before and after the introduction of low profile winglets and thus further increasing the lift/drag factor. Winglets

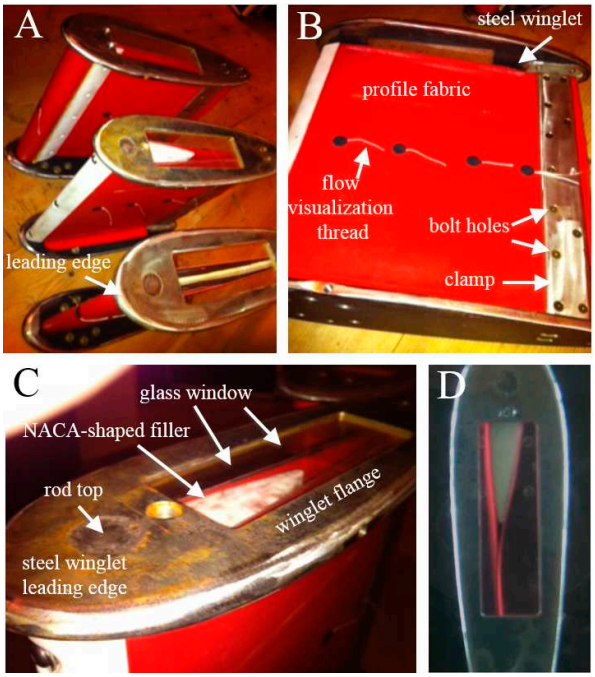

Fig. 3. TA side view of a model profile. Scale bar = 10 cm.

on the flexible profiles were therefore implemented into the full-scale turbine by combining this feature with structural elements. Observation of local and global vortex shedding and fluid flow behavior over the profiles during tests was performed with the help of strips on the surface of the wings. This was especially helpful around $0° \pm 3°$ angle of attack and at high angles of attack. It also assisted in determining the optimal fabric tension and the configuration and design of the inner structural profile elements.

2. HYDRODYNAMIC MEASUREMENT OF PROFILES WITHIN A CAVITATION TUNNEL

Measurements of lift, drag, momentum, and angle of attack for a number of profiles were performed by SSPA at Chalmers University, Goteborg, Sweden in a cavitation tunnel on a set of scale models. The SSPA cavitation tunnel high-speed section for measurements had a 1 m diameter cross-section, 23 m/s maximum speed capacity (v_0), and a 0.05 minimum cavitation number (θ) for an empty tunnel. The practical limits varied depending on how the test object was shaped and the type of test arrangement. Previous experience suggested a practical upper limit of 16 m/s tunnel speed for similar applications. The lower limit of 6 m/s tunnel speed was required to ensure sufficiently high accuracy of the

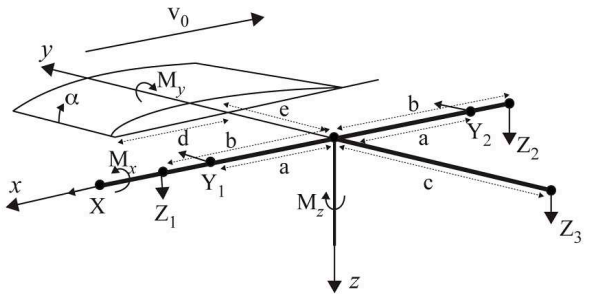

Fig. 4. The six-component parameters measured continuously during testing: $F_x = X$, $F_y = Y_1 + Y_2$, $F_z = Z_1 + Z_2 + Z_3$, $M_x = -Z_3 \cdot c$, $M_y = (Z_2 - Z_3) \cdot b$, $M_z = (Y_2 - Y_1) \cdot a$, $a = 270$ mm, $b = 300$ mm, $c = 500$ mm

force measurements and required water lubrication of the tunnel pump impeller bearings. Most tests were performed at 4 m/s or 6 m/s, with one test also performed at 8 m/s.

The profile models were attached to a six-component balance unit (SSPA designation R41) mounted in a window of the measurement section (fig. 2). An existing covering plate was used to form a flat surface between the profiles and the wall of the measurement section. The six-component balance unit was mounted at the top of the cavitation tunnel with the profile span oriented vertically. Before the test, the six-component balance was calibrated by SSPA. A principal drawing of the six-component balance is shown in fig. 4.

The transducer signals (in volts) measured during testing were low-pass filtered at 0.25 Hz, with 2 Hz sampling frequency during 15 s. The average of each signal was stored in data files. Each test was repeated twice. The same cavitation tunnel temperature, water velocity, and pressure conditions were applied to all tests. The stored voltages were converted to forces using a calibration table. The forces and moments were calculated according to the definitions in fig. 4. For calculation of the non-dimensional coefficients of lift, drag, and pitching moment, the following definitions were applied. Drag force (D), lift force (L), and pitching moment (M) (all in N/m) per unit length (l) of hydroprofile span were defined as follows: $D = -F_x/l$; $L = -F_z/l$; $M = M_y/l$. Resistance characteristics were given by the coefficients for the section drag (C_D), lift (C_L), and moment (C_M) as follows:

$$C_D = \frac{D}{\frac{1}{2}\rho V_{mf}^2 C},$$

$$C_L = \frac{L}{\frac{1}{2}\rho V_{mf}^2 C},$$

$$C_M = \frac{M}{\frac{1}{2}\rho V_{mf}^2 C}.$$

The density of water (ρ) was set to 1000 kg/m3, and the inflow velocity (V_{inf}) was set at 4, 6, and 8 m/s. The profiles were tested at atmospheric pressure and cavitation performance was not analysed but visually observed and investigated. The cavitation number (σ) in the measurement protocols (used for cavitation scaling) was defined as

$$\sigma = \frac{P_0 - P_v}{\frac{1}{2}\rho V_0^2},$$

where P_0 is the pressure of undisturbed water, P_v is the vapor pressure of water, and $v_0 = V_{inf}$, i.e. the velocity of undisturbed water.

3. DEFORMATION MEASUREMENT ON FLEXIBLE MODELS

Fabric deformation, global deflection, and tension are vital components in the behavior of flexible profiles. At high water velocity, the pre-adjusted tension, flexibility, and deformation of the fabric over time will influence the lift, drag, and momentum of the profile. Hence, the flexible materials were pre-stretched and set to ensure no additional movement would occur as a function of time and forces applied. A small frame was built to measure both fabric deformation and to adjust the fabric tension (fig. 5, *a*). A battery powered weight cell transducer (type DFI; AEP, Cognento, Italy) was used to measure the fabric tension by pulling the fabric back and fastening the trailing edge with low drag screws. Fabric tension was adjusted to 60 kg or 80 kg weight. The same frame was then moved to the top of the profile to measure the deformation of the fabric by pressing a steel rod down on the fabric and then measuring the deformation distance before and after each cavitation tunnel test (fig. 5, *b*).

4. CAVITATION TUNNEL TEST RESULTS

The cavitation tunnel test results showing the effect of profile thickness and tension force on elastic deformation of a profile are summarized in table 1. The drag increased with profile thickness and the thicker profiles usually had higher lift at lower angles of attack, agreeing with standard findings from other hydrodynamic tests. The thicker profiles also tended

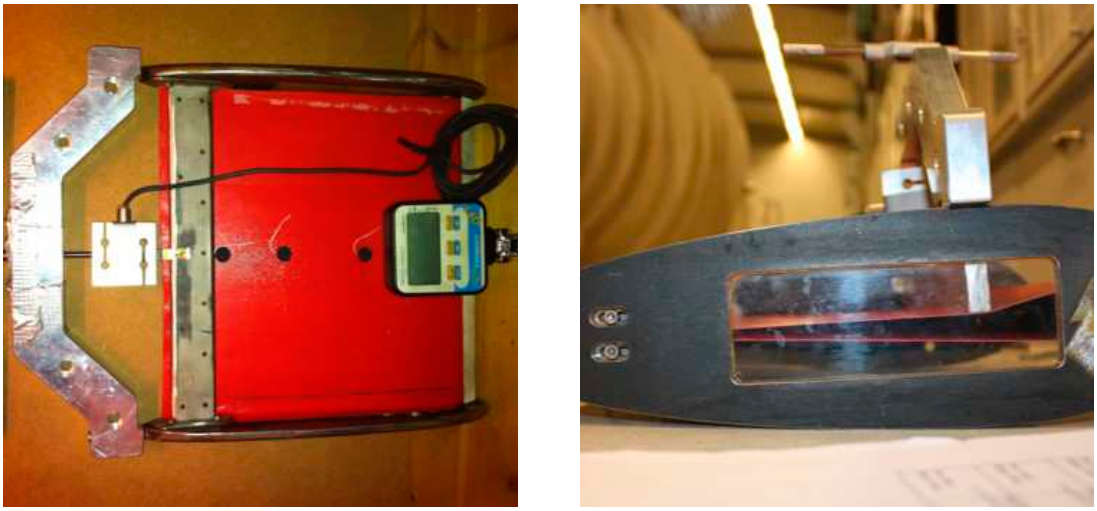

а *б*

Fig. 5. Frame used to adjust the fabric tension (a) and measure fabric deformation (b) of the model profiles

Table 1. Test program and recorded measurements for force-dependent elastic behaviour at attack angles (α) from -3° to $+32^\circ$ maximum.

Test series	LE thickness relative to chord length (%)	Tension force at TE before test (kg)	Area before test (mm^2)	Elastic deformation with 8 kg load (mm)		Comments
				Before test	After test	
1	7	6	81.200	9	–	
2	7	6	81.200	9	–	LE rod welding broke
3	10	5	83.790	16	21.5	
4	13	5	85.260	13.5	–	LE rod welding broke
5	7	50	85.260	8	10	
6	10	50	85.260	11.5	13.5	
7	13	25	86.730	10	13.1	
8	10	25	84.966	13.5	15.5	
9	13	50	92.316	7	10	
10	10	60	89.964	10	12.5	With 'nose'
11	7	60	82.940	7.1	9.3	
12	7	60	87.025	3	4.5	Partly filled
13	10	60	86.142	–	–	Partly filled
14	13	80	91.140	–	–	Partly filled
15	10	80	89.628	–	–	With 'nose' and side flaps
16	7	80	89.082	–	–	Flex NACA 0011
17	13	80	92.610	–	–	Mono

to stall earlier at higher angles of attack, although the flexibility in the profile delayed such stall compared to experience with solid profiles. The profiles with higher fabric tension (80 kg) gave lower drag due to a reduced tendency for local vortex formation that would cause non-linear flow and/or global or local

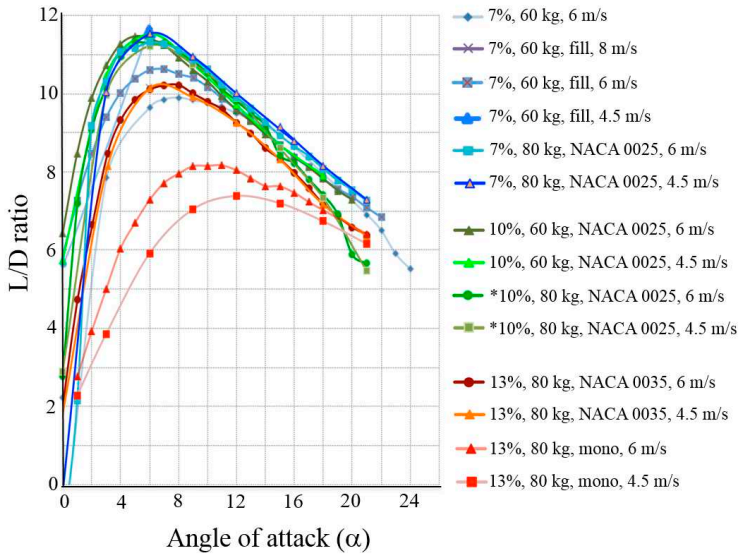

Fig. 6. Lift/drag ratio of the profile in dependence on the attack angle for various tension

stall. The profile with low fabric tension (60 kg) had higher L/D ratios at low angles of attack, but high fabric tension (80 kg) maintained high L/D ratios over a broader range of angle of attack, thus addressing the application requirements (fig. 6).

Profile designs without an internal support structure resulted in a negative pressure between the two sides of the profile, semi collapsing the two fabric pieces together and creating a negative parable behind the leading edge (fig. 7). This enhanced the vortex and turbulence created by the profile, increasing the profile's drag. Drag was reduced for profiles with internal filler or an internal profile that avoided compression induced by the negative pressure inside the profile section, and an internal support structure profile in the main hydrodynamic profile envelope gave good overall performance addressing these effects. Drag induced from nuts and bolts at the trailing edge was mechanically optimized based on studies of drag from surface imperfections by Hoerner [8]. The add-on 'nose' that was introduced into a set of tests had little effect on the lift and drag performance, while the influence of the point of zero momentum was more significant. Thus, the nose feature was not included in the final design due to its limited effect and increased design complexity for the full-scale pilot.

Structurally, a leading edge with $<$ 10% thickness/chord ratio will provided poor mechanical strength on a vertical axis tidal turbine, in particular with respect to profile structural fatigue.

A medium-high to high tension (60-80 kg) was selected to achieve a high L/D ratio over a wide range of angle of attack. This would also give lower drag and a reduced tendency for vortex formation to cause nonlinear flow and/or global or local stall. Fabric stiffness significantly affected the L/D ratio because of induced turbulence along the profile, which leads to a low L/D ratio. The fabric stiffness will also affect the self-starting abilities of the turbine, which has to be considered when determining the selected fabric tension. Thus, the final selection was a medium-high tension at 80 kg that minimized induced turbulence, as shown in series 14 (table 1). The trailing edge was designed to incorporate a tensioning arrangement that allowed adjustment. This feature was therefore included in the full-scale turbine design. The double-cambered flexible profiles showed a high capability in handling large angles of attack and a good (slow) L/D linear decay versus angle of attack, which would delay any profile stall and provide an improved general torque performance. This aspect is of particular importance for vertical axis turbines operating at low tip speed ratios with significant changes in flow angle of attack versus the rotational azimuth angle.

With increasing angles of attack, C_D and C_L increased while C_M decreased. The L/D ratios increased from 0-5 angles of attack and thereafter decreased, with the highest L/D ratios at $5-7$ angles of attack. Important features on a wing of a vertical axis tidal turbine thus include (i) high L/D ratios over a wide range of angle of attacks, (ii) sufficient mechanical strength for fatigue purposes, (iii) an integrated internal profile support that prevented

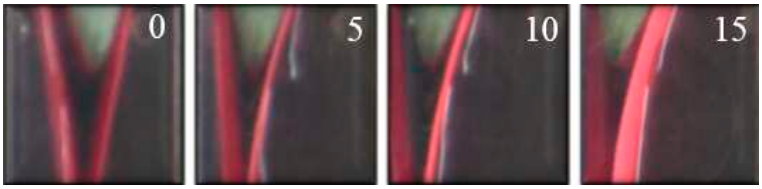

Fig. 7. A profile lacking an internal support structure profile shows the effect of negative pressure collapsing the two pieces of fabric together to form a negative parable behind the leading edge. The lower image shows the outline of the profile model. The large circle behind the leading edge is the outline for the mounting bracket for the connection to the cavitation tunnel. Scale bar = 10 cm.

Table 2. Influence of attack angles on lift and drag (with AR correction factors) for profile series 14.

α	$\frac{C_{L_{AR=3}}}{C_{L_{AR=1}}}$	$\frac{C_{D_{AR=3}}}{C_{D_{AR=1}}}$	$\frac{[L/D]_{AR=3}}{[L/D]_{AR=3}}$
5	1.73	1.17	1.49
10	1.73	1.33	1.30
15	1.73	1.28	1.36
20	1.73	1.18	1.47

local cavitation along profiles, whereby vortices from the front created a vortex dimple in the profile, and (iv) a simple design without special complexities like noses.

5. ASPECT RATIO

The aspect ratio (AR) was analyzed to apply the profile model test results into the final full-scale turbine design. The AR of the wing is defined as the ratio of the square of the span to the plan form area of the profile. The model profiles were manufactured with an AR of one, scaling up the wing will alter the aspect ratio and must be accounted for. Results from Larsson and Eliasson [9] were used to estimate the influence of AR values on the full-scale model profiles. A comparison between AR = 1 and AR = 3 for the series 14 profile (table 2) showed similar results as found in Abbot and von Doenhoff [10]. However, the results in table 2 are for typical three-dimensional profiles, while the use of end plates in the tested model profiles reduced this influence by making the profiles more two-dimensional, and hence smaller corrections could be applied. The drag of the models was higher than expected, likely because of the design of the clamping device on the aft part of the model profiles. Estimations for the drag of bolts and rivets (Hoerner [8]) were used for adjustment of the numbers used in the profile design of the full-scale turbine.

ACKNOWLEDGMENTS

We thank Jan Hallander and Torleif Johansson at SSPA (Chalmers University, Gøteborg, Sweden) for assistance with the profile design and use of their cavitation tunnel equipment. We also thank Kinetic Energy a.s. (Oslo, Norway) and the Norwegian Government Renewable Energy Program for financial support, and Dr. Carol Wenzel (Vancouver, Canada) for editing.

1. *Yamamoto I., Terada Y., Nagamatu T., Imaizumi Y.* Propulsion system with flexibile rigid oscillating fin // IEEE Journal of Oceanic Engineering.– 1995.– **20**.– P. 23–30.
2. *Katz J., Weihs D.* Hydrodynamic propulsion by large amplitude oscillation of an airfoil with chord wise flexibility // Journal of Fluid Mechanics.– 1978.– **88**.– P. 485–497.
3. *He G. Y., Zhang S. G., He G. W.* A numerical investigation of controllably flexible hydrofoil in laminar flows // Proceedings of the Fifth International Conference in Fluid Mechanics on "New Trends in Fluid Mechanics Research"..– Shanghai, China, August 15-19, 2007, Shanghai, China: Tsinghua University Press and Springer, 2007.– P. –.
4. *Shin S., Kim H. T.* Numerical simulation of fluid-structure interaction of a moving flexible foil // Journal of Mechanical Science and Technology.– 2008.– **22**.– P. 2542–2533.
5. *Milne J. G.* The Effect of Twist on Flexible Hydrofoils // Master of Applied Science Thesis.– Vancouver, Canada: University of British Columbia, 1972.– P. –.
6. *Bertin J. J., Cummings R. M.* Aerodynamics for Engineers.– Upper Saddle River, N.J., U.S.A: Pearson Prentice-Hall, 2009.– p.
7. *Anderson J. D.* Fundamentals of aerodynamics.– Boston, Massachusetts, USA: McGraw-Hill, 2007.– p.
8. *Hoerner S. F.* Fluid-Dynamic Drag. Practical Information on Aerodynamic Drag and Hydrodynamic Resistance. 2nd edition.– Brick Town, NJ, USA: Hoerner Fluid Dynamics, 1965.– p.
9. *Larsson L., Eliasson R. E.* Principles of Yacht Design. 2nd edition.– London, U.K.: Adlard Coles Nautical, 2000.– p.
10. *Abbot I. H., von Doenhoff A. E.* Theory of Wing Sections.– Mineola New York, U.S.A: Dover Publications, 1959.– p.